ACI STRUCTURAL JOURNAL TECHNICAL PAPER

Title no. 101-S78

Performance of Bridge Deck Link Slabs Designed with Ductile Engineered Cementitious Composite

by Yun Yong Kim, Gregor Fischer, and Victor C. Li

This paper presents an experimental study on the monotonic and fatigue behavior of a link slab designed for a durable concrete bridge deck system. The requirements on the link slab in terms of material properties, dimensions, and reinforcement detailing are considered. Special focus is placed on the deflection capacity of the link slab and its fatigue performance. This paper discusses the choice of a fiber reinforced engineered cementitious composite (ECC) material based on the performance requirements of link slabs in the context of an integrated structure-material design scheme. Experimental results of monotonic and subsequent cyclic tests of full-scale ECC link slabs are compared with those of an ordinary reinforced concrete link slab. The mode of deformation will be discussed with particular emphasis on the development of crack widths, which is important for durability against steel reinforcement corrosion. The significant enhancements of deflection capacity and crack width control in ECC link slabs suggest that the use of ECC material can be effective in extending the service life of repaired bridge deck systems.

Keywords: crack control; deformation; durability; fatigue.

INTRODUCTION

Many highway bridges are composed of multiple span steel or prestressed concrete girders simply supported at piers or bents. The girders support cast-in-place concrete decks. A mechanical joint is typically employed at the end of the simple span deck to allow deck deformations imposed by girder deflection, concrete shrinkage, and temperature variations. It is well known that bridge deck joints are expensive to install and maintain. Deterioration of joint functionality due to debris accumulation can lead to severe damage in the bridge deck and substructure. The durability of beam ends, girder bearings, and supporting structures can be compromised by water leakage and flow of deicing chemicals through the joints. A significant negative economic impact of mechanical joints in all phases of bridge service life, from design to construction and maintenance, was documented by Wolde-Tinsae and Klinger.[1] A possible approach to alleviate this problem is the elimination of mechanical deck joints in multispan bridges.

Two solutions to eliminate deck joints have been attempted in the US, specifically, an integral construction concept with girder continuity and a jointless bridge deck concept with simply supported girders. Alampalli and Yannotti[2] found that the jointless deck construction practice is generally more efficient than the integral bridge construction practice. Based on field inspection of 105 jointless bridge decks, including 72 with concrete superstructures and 33 with steel superstructures, it was found that the bridges were functioning as designed without significant problems except for minor deck cracking. While further improvement on jointless bridge deck construction practices was recommended, Alampalli and Yannotti concluded that as a group, they generally perform better than decks with joints.

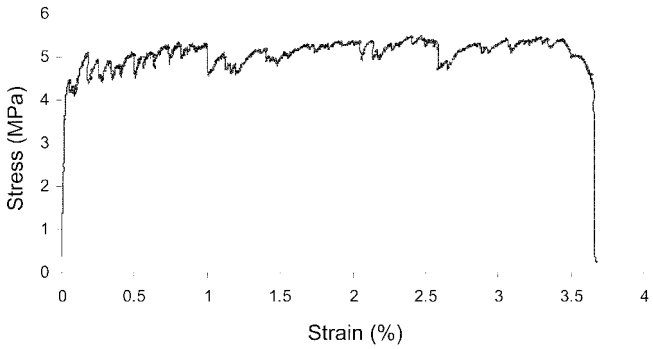

Fig. 1—Typical tensile strain-stress behavior of the ECC designed for link slab application.

The section of the deck connecting the two adjacent simple-span girders is called the link slab. Caner and Zia[3] experimentally analyzed the performance of jointless bridge decks and proposed design methods for the link slab. These investigations revealed that the link slab was subjected to bending under typical traffic conditions rather than axial elongation. Tensile cracks were observed at the top of the link slab under service conditions due to a negative bending moment. For steel girders, the measured maximum crack width was 300 μm at 40% of ultimate load and 750 μm at 67% of ultimate load. They pointed out that additional tensile stress may be imposed on the link slabs due to shrinkage, creep, and temperature loading, and that crack width must be carefully controlled. The recommendation was to use epoxy coated reinforcing bars in the link slab to avoid reinforcement corrosion. To reduce the stiffness of the link slab, debonding of the link slab over the girder joint for a length equal to 5% of each girder span was also recommended. This link slab concept can be used for new bridge decks and also for replacement of deteriorated joints of existing bridge decks.

Engineered cementitious composite (ECC) is a high-performance, fiber-reinforced cementitious composite designed to resist tensile and shear force while retaining compatibility with normal concrete in almost all other respects.[4] Figure 1 shows the uniaxial tensile stress-strain curve of an ECC reinforced with polyvinyl alcohol (PVA) fiber. After first cracking, the composite undergoes plastic yielding and strain-hardening to a tensile strain of 3.7% prior

ACI Structural Journal, V. 101, No. 6, November-December 2004.
MS No. 03-156 received May 5, 2003, and reviewed under Institute publication policies. Pertinent discussion including author's closure, if any, will be published in the September-October 2005 *ACI Structural Journal* if the discussion is received by May 1, 2005.

Yun Yong Kim *is a research assistant professor in the Department of Civil and Environmental Engineering at Korea Advanced Institute of Science and Technology, Daejeon, Korea. His research interests include the design of fiber-reinforced cementitious composites and their structural applications, including durable retrofit of infrastructures.*

Gregor Fischer *is an assistant professor in the Department of Civil and Environmental Engineering at the University of Hawaii, Manoa. He received his PhD from the University of Michigan, Ann Arbor. His research interests include the material design and structural applications of fiber-reinforced cementitious composites, and durability and repair of infrastructures.*

ACI member **Victor C. Li** *is a professor in the Department of Civil and Environmental Engineering at the University of Michigan, Ann Arbor. He is a member of ACI Committee 544, Fiber Reinforced Concrete. His research interests include the design of ultra-ductile and green cementitious composites, their application to innovative infrastructure systems, and integration of materials and structural design.*

to developing a macroscopic crack. The tensile strain capacity of ECC is about 370 times that of normal concrete. ECC achieves strain-hardening with moderate amounts of fibers (typically less than or equal to 2% by volume) compared with other high-performance fiber-reinforced concrete. This is particularly important for practical field applications, where the mixing process must be simple and similar to that used in mixing and placing conventional concrete. As confirmed by studies on self-compacting ECC[5] and sprayable ECC,[6] the fresh properties of ECC can be adjusted by optimizing the composition for given workability requirements. Thus, the introduction of ECC to link slab construction is proposed for its ability to control crack widths and its processing flexibility.

The purpose of this paper is to demonstrate the performance of link slabs designed with ductile ECC material for macroscopically crack-free concrete bridge decks. In the selection of ECC material, the property requirements on the link slab material as well as processing demands were considered. The performance of ECC link slabs was evaluated by testing full-scale sections of link slab specimens. The test results were compared with those of an ordinary reinforced concrete (RC) link slab. The mode of deformation, fatigue cracking resistance, and design of link slab associated with the development of reinforcing bar stress and crack width will be discussed.

RESEARCH SIGNIFICANCE

In this study, monotonic and fatigue performances of ECC link slabs are evaluated and compared with those of ordinary concrete link slabs. An ECC material is chosen based on an integrated structure-material design scheme as well as on workability. Specifically, the significance of this investigation lies in the potential realization of macroscopically crack-free concrete bridge deck systems due to the tensile strain capacity of ECC material, compatible deformation of ECC with reinforcing bars, and tightly controlled crack widths of ECC in the link slabs. The use of ECC link slabs is expected to provide a durable jointless bridge deck with significantly reduced maintenance requirements compared with conventional jointed concrete bridge decks or bridge decks with link slabs constructed from ordinary RC.

PROPERTY REQUIREMENTS OF ECC MATERIAL FOR LINK SLABS

For material selection based on the integrated structure-material design concept,[7] property requirements of ECC material for link slabs were examined prior to material design. As a minimum compressive strength, 35 MPa was adopted on the basis of widely chosen design compressive

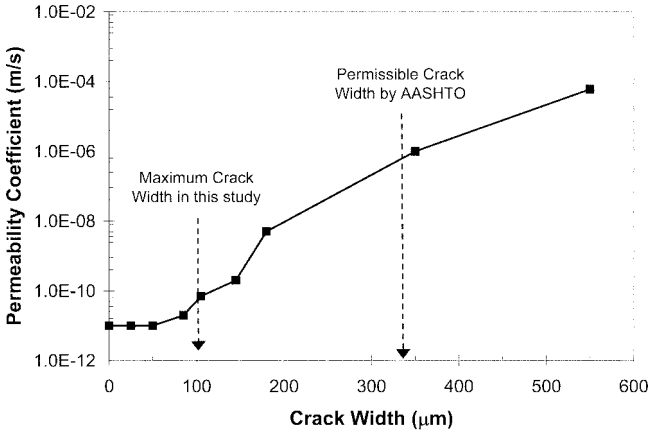

Fig. 2—Permeability coefficient as function of crack width.[9]

strength (27.5 MPa) of concrete in bridge deck slabs. Current AASHTO Standard Specifications for Highway Bridges 2002[8] (AASHTO code hereafter) provide a maximum permissible crack width of 330 μm in RC bridge decks in severe exposure conditions. The influence of reduced crack width on the permeability of water contaminated by harmful substances such as chlorides introduced by deicing salt can be evaluated using reference data.[9] The data in Fig. 2 indicates that for crack widths below 100 μm the permeability coefficient remains relatively small and constant (10^{-10} m/s). At increasing crack widths, however, the permeability coefficient increases rapidly and reaches values several magnitudes higher (10^{-6} m/s at 330 μm crack width). Therefore, the desired crack width was minimized to less than 100 μm to approach transport properties of sound concrete without cracks for corrosion resistance.

Assuming 5% debond length L_{ls} between deck and girder, at each end of a bridge span of length L_{sp}, the strain capacity ε_{ls} of the ECC link slab needed to accommodate the movement imposed by $\Delta T = 50$ °C temperature variations and shrinkage strain ε_{sh} (~0.1%)[10] and the maximum tensile strain ε_{LL} (< 0.1%)[11] in the link slab due to the imposed bending moment from the end rotations caused by live loading of adjacent spans can be estimated as follows

$$\varepsilon_{ls} = \frac{\alpha_T \cdot \Delta T \cdot L_{sp}}{L_{ls}} + \varepsilon_{sh} + \varepsilon_{LL} = \tag{1}$$

$$\frac{0.000012 \cdot 50 \cdot L_{sp}}{0.1 \cdot L_{sp}} + 0.001 + 0.001 \approx 0.8\%$$

where α_T is the coefficient of thermal expansion of concrete and steel. With a safety factor of two, the minimum required tensile strain capacity of ECC material was estimated to be 1.6% for link slab applications.

MATERIAL COMPOSITION AND PROPERTIES

The ECC material used for link slab specimens used 2% by volume of PVA fibers tailored based on micromechanical principles,[4] Type I ordinary portland cement, fine aggregates (particle diameter = 110 ± 14.8 μm), Type F fly ash, water, and a water-reducing admixture. The mixture proportion of the ECC employed in this study is given in Table 1. Material properties obtained from this composition at the age of 28 days

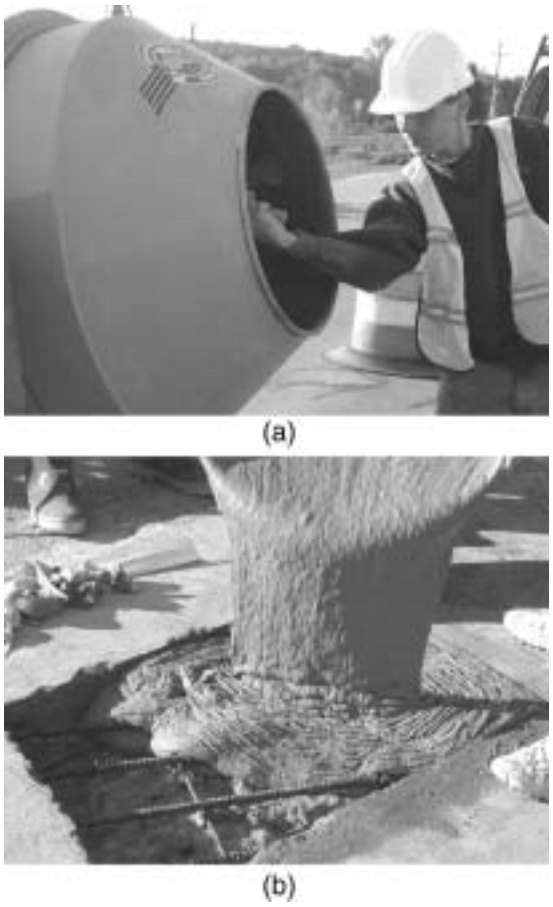

Fig. 3—Demonstrations of ECC workability in patching of bridge deck for: (a) mixing in 340 L capacity drum mixer; and (b) pouring without any vibration.

Table 1—Mixture proportion of engineered cementitious composite employed in this study

Cement	Water	Sand	Fly ash	High-range water-reducing admixture*	Fiber volume fraction V_f
1.00	0.53	0.80	1.20	0.03	0.02

*High-range water-reducing admixture dosage equal to 29 lb/yd^3.
Note: All numbers are weight ratios except for fiber volume fraction V_f.

were a first crack strength of 4.0 MPa at approximately 0.02% strain and an ultimate tensile strength of 6.0 MPa at 3.7% strain (Fig. 1). The tensile strain hardening behavior and multiple cracking with crack widths below 100 μm provided an allowable performance level for the ECC. The compressive strength of ECC was 80 MPa at 28 days and significantly higher than anticipated (35 MPa). This indicates that the hardened properties of the ECC can meet and exceed the structural requirements of link slabs. The expected maximum imposed strain (1.6% with safety factor of two) is in the early strain-hardening regime of this ECC with microcrack widths maintained below 100 μm. These ECC properties will provide link slabs with significantly enhanced rotational and axial deformation capacity while controlling crack width, resulting in low permeability and reduced maintenance needs of repaired bridge deck systems with ECC link slabs.

In addition to the hardened properties, the mixing process and workability are also critical for practical applications.

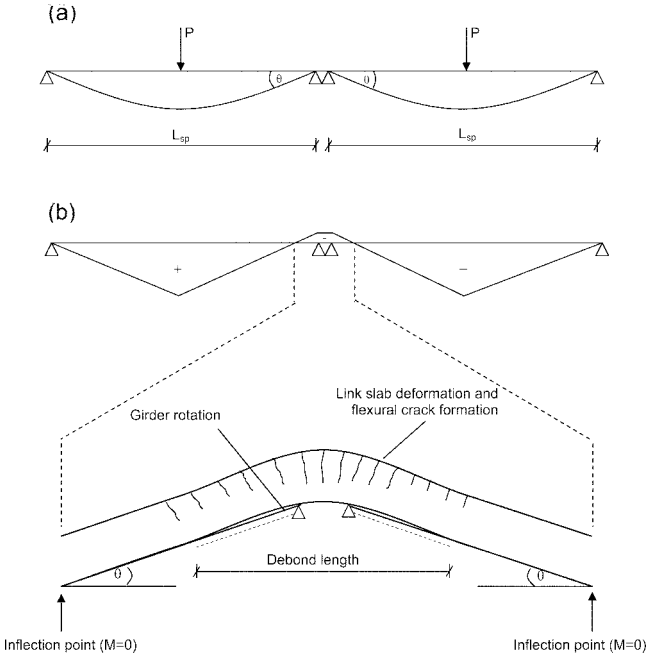

Fig. 4—Schematics of two-span bridge subjected to point load at midspan for: (a) deformed shape of bridges; and (b) moment distribution on bridge span and corresponding deformed shape of link slab region.

The fresh property of the ECC employed in the present study was demonstrated in a bridge deck patching. The ECC was mixed in a 340 L capacity drum mixer (Fig. 3) and then placed into the patch. The ECC patch was hand finished with steel trowels to a smooth surface followed by tining to create transverse grooves in the surface. It was found that ECC exhibited excellent workability eliminating the need for vibration between the reinforcing steel and moderate finishability as well. Durability performance resisting freezing-and-thawing will be discussed in a follow-up paper.

A ready-mixed concrete was used for the concrete link slab and adjacent bridge deck, which served as the control specimen. The compressive strength of concrete was 35 MPa at 28 days. Tensile test on concrete was not carried out, but the concrete was assumed to have a tensile strength of 3 MPa at 0.01% strain.

EXPERIMENTAL PROGRAM

Testing configuration

While previous laboratory investigation of link slabs[3,11] involved testing of a 1/6-scaled bridge including a link slab with two adjacent spans, the present study focused on testing of a full-scale link slab portion exclusively. Therefore, the end rotations imposed on the link slab by the adjacent spans in a bridge were replicated in the laboratory.

The deformed shape and moment distribution due to applied load of a two-span bridge structure are schematically shown in Fig. 4(a). Flexural crack formation was expected at the top of the link slab as illustrated in Fig. 4(b). Therefore, the link slab specimens were designed to include the link slab within the distance between the points of inflection in the adjacent spans. The location of inflection points should be determined by the stiffness of the link slab. In case of zero stiffness, the point of inflection is located at the support, while for a continuous girder and deck its location is at 20% of the span length from the support. In the case of a link slab

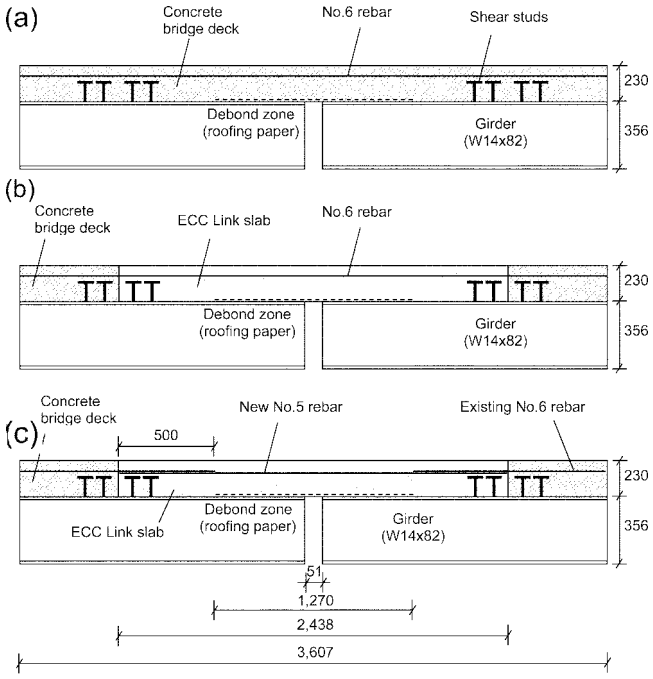

Fig. 5—Geometry of link slab specimens for: (a) LS-1; (b) LS-2; and (c) LS-3. (Dimensions shown in mm.)

with girder discontinuity, the point of inflection is located within these boundaries.

Design of test specimens

As described previously, the specimen test setup focused on the link slab portion between the points of inflection in the adjacent spans as illustrated in Fig. 4(b). Figure 5 shows the specimen geometry of both a concrete and ECC link slab, including the debond zone length (1.27 m) equal to roughly 2.5% of both adjacent spans. It is noted that the length and height dimensions of the specimens are identical to a link slab between two adjacent 25 m span bridges. The thickness of the link slab was 230 mm, which corresponds to typical deck slabs in simply supported composite girder bridges. As described previously, the location of the inflection point should be located in the range from 0% up to 20% of the span. We employed an inflection point at 7% of the span based on a numerical analysis procedure.

Three link slab specimens (Fig. 5) were tested. Specimen LS-1, in which a concrete link slab reinforced with continuous No. 6 reinforcing bars and adjacent spans were cast together, was used to simulate the concrete link slab new construction. According to the current limit stress criterion of RC link slabs,[3] the reinforcement ratio of the concrete link slab was determined to satisfy the stress criterion ($\sigma_s < 0.40\ \sigma_y$) at a 0.0015 rad end rotation angle. This is the expected rotation angle as derived by Caner and Zia.[3] The moment $M_{a,g}$ developed in the uncracked concrete link slab is a function of the elastic modulus of concrete E_c and geometrical dimensions. It is proportional to the imposed end rotation angle θ.

$$M_{a,g} = \frac{2E_C I_{ls,g}}{L_{ls}}\theta \qquad (2)$$

where $I_{ls,g}$ is the second moment of inertia of the link slab based on an uncracked section and L_{ls} is the debond length. Figure 6 illustrates the stress in the reinforcement at a 0.0015 rad

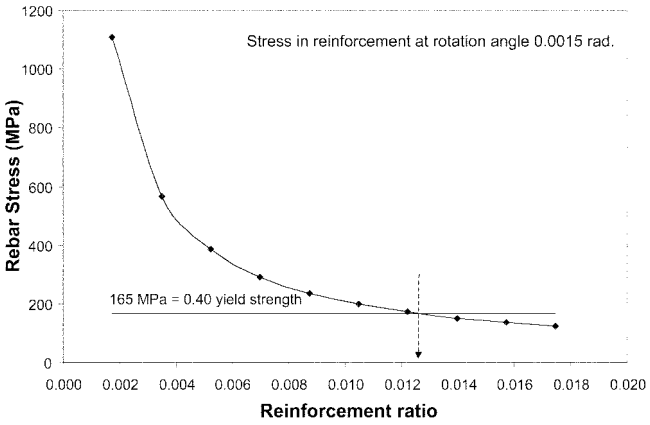

Fig. 6—Reinforcement ratio 0.014 designed at expected rotation angle (0.0015 rad).

end rotation angle and the reinforcement ratio chosen in this test. In the debond zone, no shear connectors were used and 15-lb roofing paper was placed at the top of the W14x82 girder flange. Specimen LS-2 was prepared by removing the concrete from the link slab portion of Specimen LS-1 and replacing it with an ECC link slab. This specimen was used to simulate the replacement of a RC link slab with a new ECC link slab since the continuous reinforcement remained. The length of the link slab was 2.44 m including 1.27 m length of debond zone. The debond zone in the conventional concrete link slab has been designed to begin at the interface between deck slab and link slab, which results in locating the interface at the weakest part of the bridge deck system. In the present study, four shear studs were welded at each end of the ECC link slab portion on the top of the girder flange (Fig. 5(b)) to strengthen the interface between the ECC link slab and RC bridge deck. The following steps were followed to prepare Specimen LS-2 after the fatigue test on Specimen LS-1:

1. Mark the section of the deck to be removed;
2. Provide a 25 mm deep saw cut across the width of the deck;
3. Chip out the concrete using a hand held pneumatic breaker; care was taken not to damage the existing reinforcements and shear studs;
4. Place formwork; the interface was located behind the four shear studs;
5. Place a layer of 15 lb roofing paper on the top flange for debonding; and
6. Pour two batches of ECC mixed in a 340 L capacity drum mixer.

To investigate the effects of the reinforcement ratio on fatigue performance of the ECC link slab, a third specimen LS-3 was prepared. Specifically, the focus of this test was on the fatigue performance of the ECC link slab reinforced with a smaller amount of reinforcement compared with the design value and the fatigue cracking resistance of an interface reinforced with the lap spliced existing reinforcing bar. As shown in Fig. 5(c), Specimen LS-3 simulates the retrofit of an existing bridge replacing mechanical joints with an ECC link slab. This specimen was prepared by removing the ECC from the link slab portion of Specimen LS-2 and pouring new ECC into the removed portion. The existing No. 6 reinforcements were cut out with 500 mm left at both ends of the link slab. These 500 mm exposed No. 6 bars were lap spliced with new No. 5 bars to simulate the retrofit of an existing bridge. A reinforcement ratio of 0.01, which is lower than that of Specimens LS-1 and LS-2, was employed as the reinforcement ratio of the Specimen LS-3.

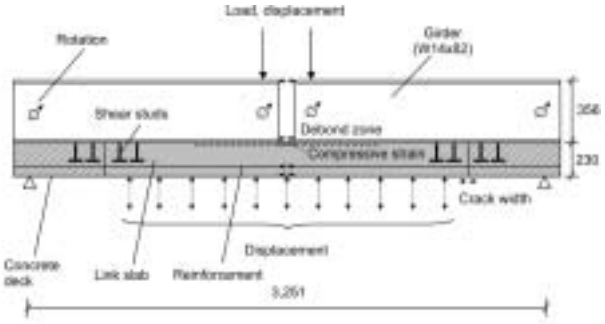

Fig. 7—Laboratory test setup and instrumentation of specimen. (Dimensions shown in mm.)

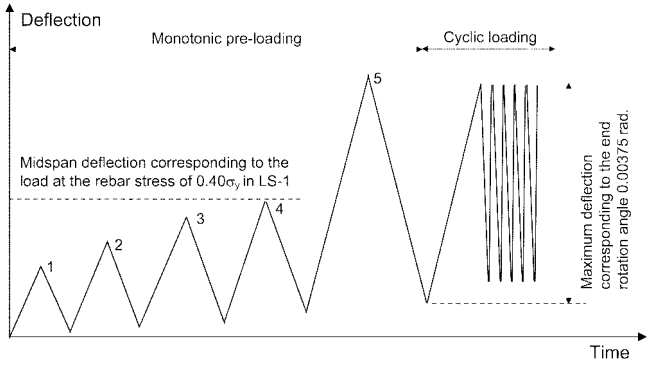

Fig. 8—Loading sequence, in which midspan deflections at Step 4 correspond to load at reinforcing bar stress equal to 0.4σ_y in Specimen LS-1.

The following steps were followed to prepare Specimen LS-3 after the fatigue test on Specimen LS-2:

1. Mark the section of the deck to be cut out;
2. Provide saw cuts across the width and depth of the deck to remove the link slab portion of Specimen LS-2 (except for the lap splice portion);
3. Mark the section of the deck to be removed and provide a 25 mm deep saw cut across the width of the deck;
4. Remove the ECC using hand held pneumatic breaker;
5. Place new reinforcing bars with 500 mm lap splice length;
6. Place formwork and a layer of roofing paper on the top flange for debonding; and
7. Mix and pour ECC into formwork to create the new ECC link slab.

Experimental test setup and procedure

The experimental investigation of ECC link slabs was conducted using a representative section (711 mm wide) of a link slab between the inflection points of the adjacent deck slabs (3.25 m long). The zero moment condition at the inflection points as well as the boundary conditions at the pier were simulated by roller supports at the specimen end supports and at the load points (Fig. 7). For practical purposes, the test setup represents an inverted orientation of the link slab region.

Table 2—Comparison between laboratory and field testing conditions

Condition	End rotation angle θ	Debond length	M_a*
Field	0.00150 rad†	5.0% of span length	M_a in field
Laboratory testing	0.00375 rad	2.5% of span length	Five times of M_a in field

*Moment developed in link slab at end rotation angle θ, based on Eq. (2).
†End rotation angle expected in field as derived in Caner and Zia.[3]

The loading sequence chosen was similar to the procedure adapted by MDOT.[11] As shown in Fig. 8, all specimens were subjected to sequential static loading up to two times the deflection causing a reinforcing bar stress in Specimen LS-1 of 40% of its yield strength, which is the current limit stress criterion for concrete link slab design. The final step of the sequential static loading stage simulates potential overload. In the subsequent cyclic loading procedure, the load at 40% yield of the reinforcement in LS-1 is chosen as the mean load with an amplitude up to a maximum deflection at 0.00375 rad rotation angle (Fig. 8). This maximum rotation angle θ_{max} (0.00375 rad) corresponds to the allowable deflection of a bridge span under live load (Δ_{max}, L_{sp}/800 in AASHTO code)

$$\theta_{max} = \frac{\Delta_{max}}{\Delta}\theta = \frac{\Delta_{max}}{PL_{sp}^3/48EI_{sp}}\frac{PL_{sp}^2}{16EI_{sp}} = \frac{L_{sp}}{800}\frac{3}{L_{sp}} = 0.00375 \text{ rad} \quad (3)$$

where L_{sp} is bridge span length and EI_{sp} is flexural rigidity of the bridge section. Cyclic loading was carried out to 100,000 cycles due to restrictions in the availability of the testing equipment. It should be noted that these test conditions are five times that assumed under field conditions in terms of the bending moment imposed by girder end rotations (Table 2).

During testing, the applied load, displacements, rotation angles, strains at the compressive face of link slab at midspan, and interfacial crack widths of the specimen as indicated in Fig. 7 are monitored using a data acquisition system. Cracks are marked and crack widths are measured using hand held crack gages at each loading sequence during the monotonic preloading procedure as well as at every 10,000 cycles during the cyclic loading procedure.

RESULTS AND DISCUSSION

Monotonic behavior of link slab specimens during preloading test

A monotonic test on the link slab specimen was conducted before fatigue testing. After this initial test, the experimental data were examined and fatigue testing was continued. For LS-1, at a midspan deflection of 1.5 mm (first step), a small transverse crack formed across the deck near midspan of the link slab. The crack width gradually grew wider during

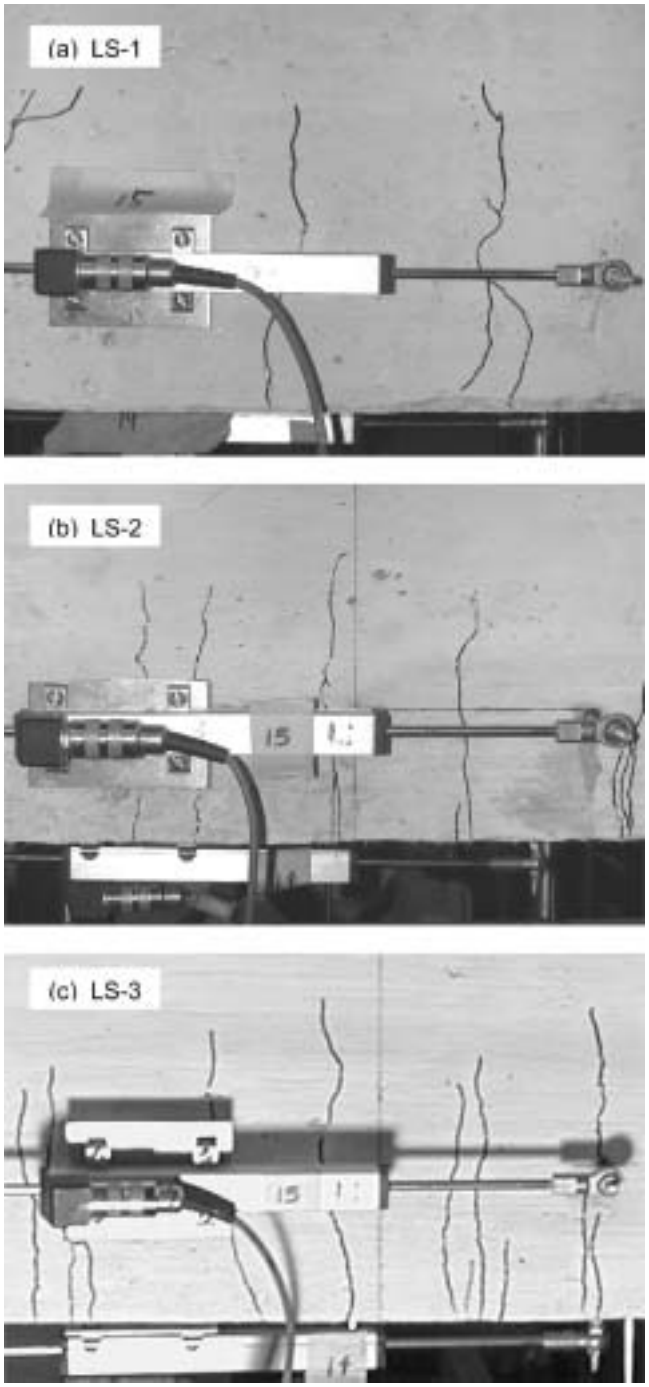

Fig. 9—Crack pattern marked with ink pen during preloading test for: (a) LS-1; (b) LS-2; and (c) LS-3 (close look inside LVDT gage length at midspan).

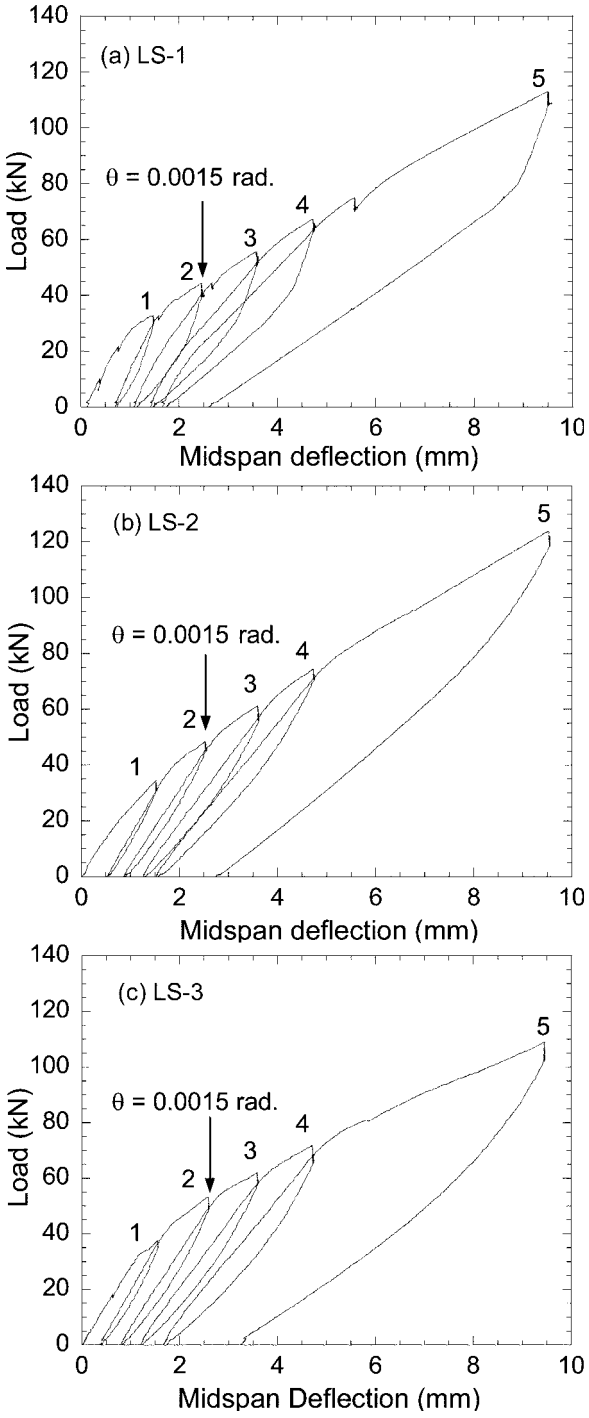

Fig. 10—Applied load versus midspan deflection curves during preloading test (Step 1: 1.5 mm; Step 2: 2.5 mm; Step 3: 3.6 mm; Step 4: 4.7 mm; and Step 5: 9.5 mm in midspan deflection) on: (a) LS-1; (b) LS-2; and (c) LS-3.

subsequent loading and reached 130 μm at the final deflection step (9.5 mm) of the monotonic preloading test. Additional cracks appeared and propagated across the width of the link slab as the midspan deflection was increased. Ultimately, seven cracks were observed during the preloading test. As shown in Fig. 9, two of these cracks formed within the gage length (230 mm) of LVDTs at midspan. One of the crack widths within the gage length was below 50 μm up to final deflection step while the largest cracks outside the gage length that developed continuously increased (~130 μm at final deflection step) as the loading step increased. In contrast to that, several microcracks appeared in the debond zone of the ECC link slabs at a midspan deflection of 1.5 mm (first step) and 2.5 mm (second step). Additional hairline cracks formed as the midspan deflection was increased (Fig. 9). All the crack widths remained below 50 μm up to the final deflection step (9.5 mm) of the preloading test.

Figure 10 shows the load versus midspan deflection curves of the three specimens tested. Significant differences in the global response of Specimens LS-1 and LS-2 are not apparent. The responses in an individual cross section, however, were distinct for the concrete and ECC link slabs.

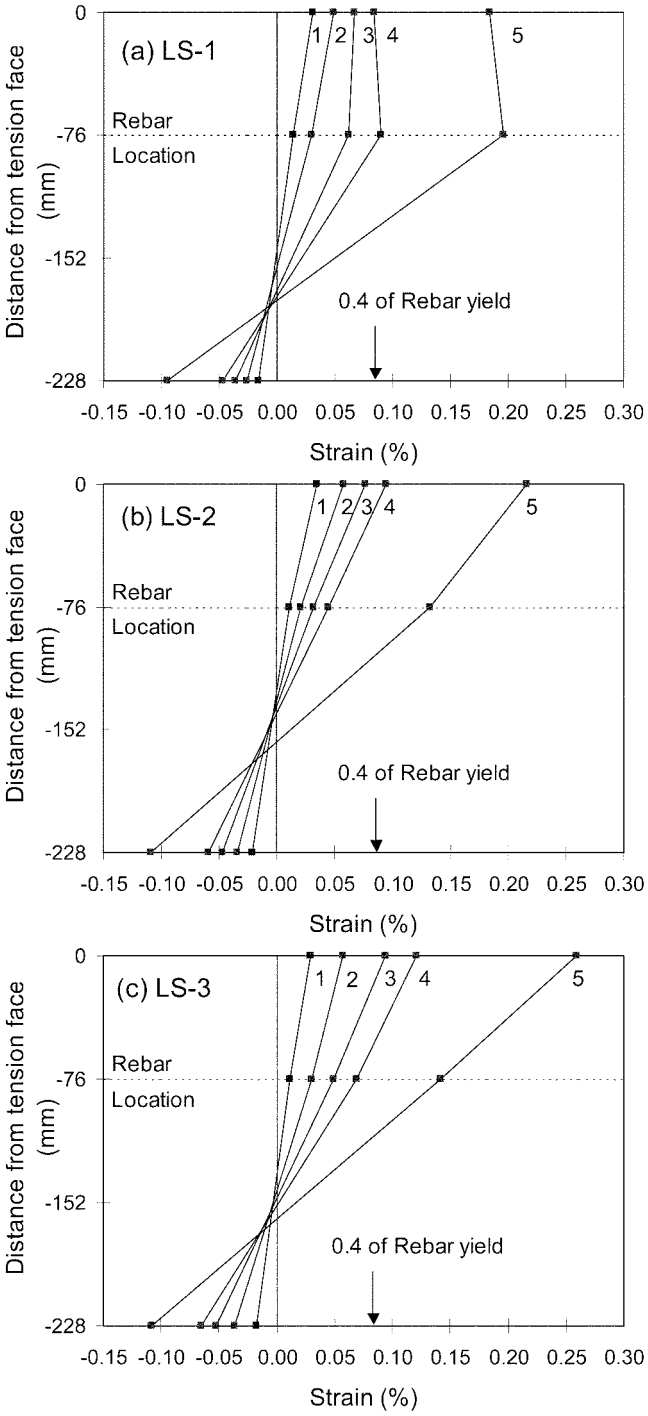

Fig. 11—Strain distribution measured at three locations (from tension surface) across midspan section at each loading step (Step 1: 1.5 mm; Step 2: 2.5 mm; Step 3: 3.6 mm; Step 4: 4.7 mm; and Step 5: 9.5 mm in midspan deflection) for: (a) LS-1; (b) LS-2; and (c) LS-3.

Figure 11 illustrates the strain distribution at three locations across the midspan section at each loading step. In this figure, the matrix strain at the tension face and the reinforcing bar strain were calculated by dividing the measured LVDT displacement by the gage length (230 mm), while strains at the compression face were obtained by averaging data measured from two strain gages placed on the compression face of the link slab at midspan. A comparison of stresses in the reinforcement at the design rotation angle 0.0015 rad

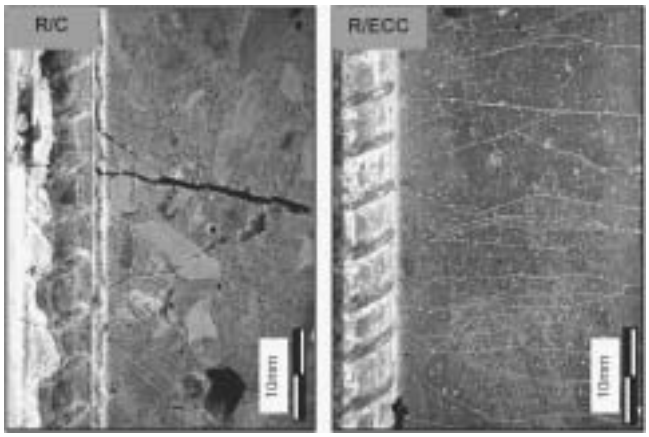

Fig. 12—Brittle fracture of concrete in normal RC (left) causes unloading of concrete, resulting in high interfacial shear and bond breakage. In contrast, compatible deformation between ECC and steel reinforcement (right) showing microcracking in ECC with load transmitted via bridging fibers.[4]

revealed the reinforcing bar strain of the ECC link Slab LS-2 (~0.02%) was smaller than that of the concrete link Slab LS-1 (~0.03%). The difference between these two reinforcing bar stresses became larger as the midspan deflection was increased. This is due to the strain hardening and microcracking of ECC material, allowing for compatible deformation of the ECC matrix with reinforcing bars as well as due to the lower stiffness of ECC as compared with concrete in compression.

A comparison of the sequential strain development at midspan section in the three specimens confirms the strain compatibility of the ECC link slabs (Fig. 11). Because of the different distances from the neutral axis of the beam, the measured strain on the tensile face (of concrete and ECC) should be higher than that in the reinforcing bar if the beam is acting elastically. At a midspan deflection of 3.6 mm (third step), the strain of the reinforcement became almost identical to the concrete strain at the tension face in Specimen LS-1. The reinforcing bar strain became even larger than the concrete strain at the tension face during subsequent loading. This indicates that the concrete in Specimen LS-1 lost compatibility with the reinforcing bars due to the localized cracks. For the ECC link slabs, the difference between the strain of reinforcement and the ECC strain at tension face was maintained in a proportional manner, that is, the three strain data points; ECC at tension face, reinforcement depth, and ECC at compression face recorded at each step can be plotted on a straight line (Fig. 11).

As shown in Fig. 12, there is basically no shear lag between reinforcing bars and the surrounding ECC material in steel-reinforced ECC (RECC) while the brittle fracture of concrete in RC causes unloading of concrete, resulting in high interfacial shear and interfacial bond failure.[4] Stress concentrations on the reinforcement are nonexistent even as the ECC is experiencing microcrack damage. Subsequently, the yielding of the reinforcing bar is delayed in the ECC matrix compared with that in the concrete matrix. In a study conducted by Fischer and Li[12] on the tension stiffening behavior of RC and RECC, strain jumps were measured locally by strain gages attached to the reinforcing bar in concrete whenever the concrete cracked, but these stress jumps were not observed in the reinforcing bar in the ECC matrix. This unique behavior is caused by ECC material exhibiting a metal-like behavior and deforming compatibly

with reinforcing bars. The microcracks (< 50 μm in widths) developed in ECC act as inelastic damage distributed over the bulk volume of ECC. In contrast, beyond the elastic limit, concrete experienced localized fracture.

Assuming the same end rotation angle θ in both RC and RECC members as seen in Fig. 13, the members must have an identical curvature Φ based on identical span length *L*, as shown in the following equation

$$\Phi = \frac{M}{EI} = \frac{2EI\theta}{L}\frac{1}{EI} = \frac{2\theta}{L} \quad (4)$$

where *M* is the moment induced by end rotation angle and *EI* is flexural rigidity. The neutral axis in RECC section is located closer to reinforcement when compared with a RC section, since ECC in tension carries force while deforming compatibly with the reinforcing bar. Due to the difference in the location of neutral axis, however, the reinforcing bar strain in RC is higher than in RECC (Fig. 13). Lower reinforcing bar stress developed in the ECC link slab indicates that the amount of reinforcement in an ECC link slab can be reduced, resulting in lower structural stiffness. This will be discussed again in the next section on the fatigue cracking resistance of link slabs.

Reinforcing bar strain (~0.03%) of the concrete link slab at the design rotation angle of 0.0015 rad did not reach 40% of the yield strain (~0.08%). This demonstrates that the assumption of the link slab in an uncracked condition caused the design moment $M_{a,g}$, based on current limit stress criterion,[3] overestimates the required amount of longitudinal reinforcement in the link slab. It should also be noted that the maximum strain at the tension face was measured to be lower than 0.1% at a design load corresponding to a 0.0015 rad end rotation angle. Considering the relative magnitude of these quantities (0.1% strain caused by end rotation, 3.7% strain capacity), the ECC material in link slabs remains in the early strain-hardening regime.

Fatigue cracking resistance of link slab specimens

Based on the monotonic test results of concrete Specimen LS-1, the load at 40% yield of the reinforcement (~70 kN) was chosen as the mean load level with an amplitude up to a maximum deflection at 0.00375 rad. Consequently, a 2.0 mm deflection amplitude was cyclically imposed on the link slab specimens. Figure 14 illustrates the response to cyclic loading as a function of midspan deflection during the test of Specimen LS-1. This specimen was loaded from 23 kN up to 105 kN with the maximum midspan deflection of 6.2 mm calculated by subtracting initial residual deflection (~2.5 mm) from total deflection (~8.7 mm). This maximum midspan deflection corresponds to the maximum rotation angle of approximately 0.00375 rad.

Cyclic test data was periodically recorded at every 10,000 cycles. The recorded data indicates that the stiffness of the specimens remained unchanged during the cyclic testing, that is, there was no global damage observed (Fig. 15). The structural stiffness of Specimen LS-3, however, was measured to be lower than those of the other two specimens, while Specimens LS-1 and LS-2 had a similar stiffness. This is due to the relatively low reinforcement ratio of LS-3, which was deliberately chosen based on relatively low reinforcing bar stress in ECC link slabs compared with the concrete link slab. Realization of low structural stiffness will be

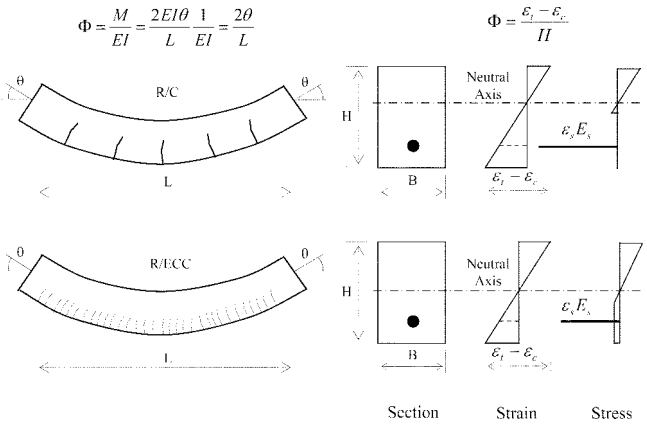

Fig. 13—Comparison of reinforcing bar stress in RC beam and RECC beam with same geometry and reinforcement ratio at identical rotation angle θ and curvature Φ.

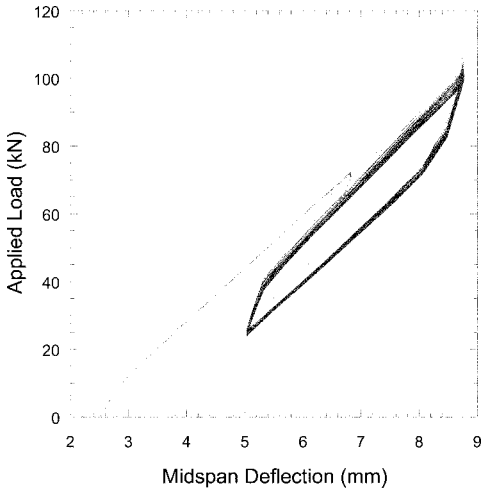

Fig. 14—Response of midspan deflection versus actuator force (applied load) behavior to cyclic deflection during cyclic test on Specimen LS-1.

an advantage of an ECC link slab since the structural effect on the main bridge span can be minimized when the link slab acts more like a hinge rather than a continuous element.

Although global damage did not occur in all the specimens, the cracking patterns were distinctly different for the concrete and ECC link slabs. For LS-1, no additional cracks were seen and the existing cracks generated during the preloading stage gradually grew wider. The crack widths in concrete ultimately reached approximately 640 μm at 100,000 loading cycles (Fig. 15). In contrast, additional microcracks appeared as the number of loading cycles increased in ECC link slab specimens (LS-2 and LS-3), while the existing crack widths were maintained below 50 μm, slightly opening and closing at the maximum and minimum loads, up to 100,000 cycles.

Figure 16 presents the comparison of the marked crack pattern between LS-1, LS-2, and LS-3. A large number of hairline cracks were observed in the ECC link slab specimens, while a small number of large cracks in Specimen LS-1 were observed. This demonstrates that fatigue cracking resistance of ECC link slabs, in terms of crack width, is independent of the reinforcement ratio because of the inherent multiple cracking and tight crack width control of ECC. Such reduced crack width and high ductility in ECC indicate the potential

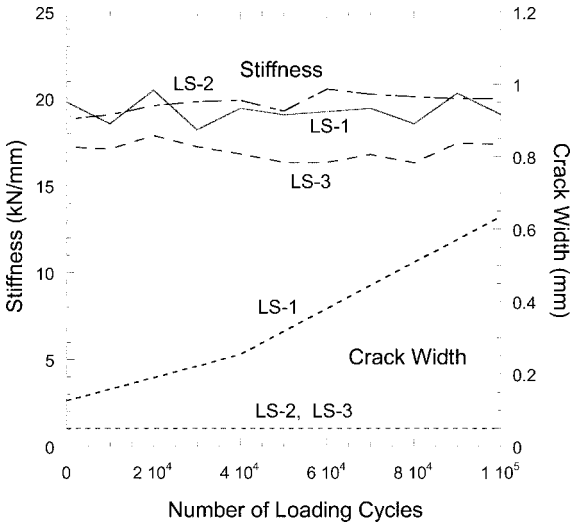

Fig. 15—Stiffness change and crack width evolution of link slab specimens during cyclic test.

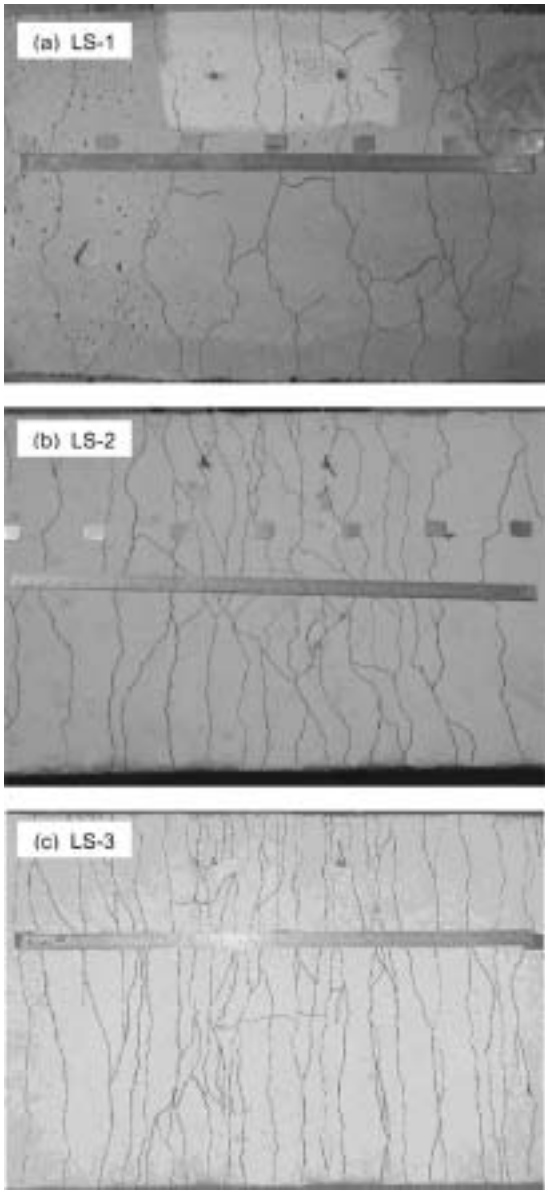

Fig. 16—Crack pattern marked with ink pen after cyclic test for: (a) LS-1; (b) LS-2; and (c) LS-3.

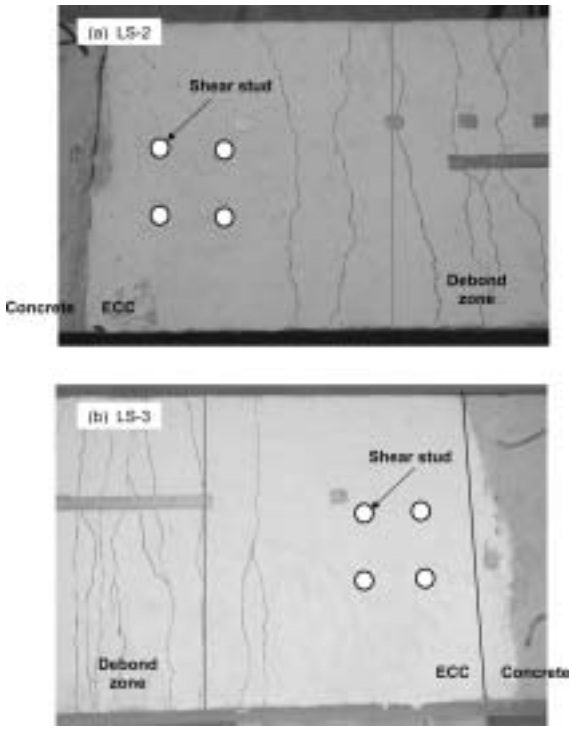

Fig. 17—Crack pattern marked with ink pen at interface zone for: (a) LS-2; and (b) LS-3.

realization of macroscopically crack free concrete bridge deck systems through the use of ECC material in link slabs. It is also expected that the low permeability of ECC due to relatively small crack widths will enhance the durability of an ECC link slab particularly under severe environmental conditions, such as in regions where deicing salts are frequently used.

Besides the stress limitation requirement described previously, the current design procedure of concrete link slab also requires limiting the maximum crack width at the top of the link slab. A minimum reinforcement ratio of 0.015 has been suggested with a clear cover of 63 mm for the purpose of controlling the crack width in the concrete link slab.[13] Therefore, the inherent tight crack width of ECC material is expected to provide a more efficient link slab design due to the decoupling of crack width and reinforcement ratio in addition to other advantages represented by enhanced durability, lower structural stiffness, and compatible deformation of ECC link slabs.

It should also be noted that there was no cracking observed at the interface between the RC deck slab and ECC link slab (Fig. 17). In contrast, cracking formed over the debond span of link slab up to the location of shear studs. This indicates that cracks should have appeared at the concrete/ECC interface if it had been located at the end of debond zone. The modification of the design to locate the concrete/ECC material interface away from the structural interface between the debond zone and girder/deck composite zone prevented cracking at the material interface. Furthermore, the additional shear studs placed between these two interfaces provided composite action between the girder and ECC slab. As a result, cracking at the concrete/ECC interface caused by stress concentrations is prevented. Instead, cracking is limited to within the bulk part of ECC, where higher strength and sufficient strain capacities exist to accommodate the higher stress. This modification of the interface from conventional link slab design will provide enhanced integrity of concrete/ECC interfaces, preventing

undesirable interfacial cracking. The link slab interface design will be further discussed in a follow-up paper.

CONCLUSIONS

To demonstrate the potential of a durable concrete bridge deck system with the use of an ECC material in link slabs, monotonic and subsequent cyclic tests of full-scale ECC link slabs were performed. The test results were compared with those of a conventional concrete link slab. Prior to the preparation of the link slab specimens, a predesigned ECC material was chosen for meeting the property requirements for link slab applications. The following conclusions can be drawn from the current experimental results:

1. Property requirements of ECC material for link slabs were examined prior to material choice. It was revealed that the property requirements for link slab applications were satisfied with the hardened properties of ECC material chosen in the present study. This ECC exhibited strain-hardening behavior with tensile strain capacity of 3.5% accompanied by multiple cracking with crack widths below 100 μm while maintaining workability suitable for large volume mixing and casting in the field;

2. Monotonic test results revealed the compatible deformation mode of the ECC link slab. The high tensile ductility of ECC material allows the ECC matrix to deform compatibly with the reinforcing bars. As a result, yielding of the reinforcing bar was delayed in the ECC matrix when compared with that in the concrete matrix. Lower reinforcing bar stress in the ECC link slab implies a smaller amount of reinforcing bars required, resulting in lower structural stiffness of the link slab. The lower reinforcing bar stress is confirmed in the ECC link slab, in comparison to the reinforcing bar stress in the concrete link slab, at the same reinforcement ratio;

3. From the monotonic tests, the maximum tensile strain in the ECC link slab measured at the design end rotation angle remained within the early strain-hardening regime. This confirmed the adequacy of the strain capacity of the ECC used in this study. Indeed, there is room to employ an ECC with slightly lower tensile strain capacity, with potential material cost saving;

4. The cyclic tests performed on three link slabs revealed that the stiffness of the three specimens remained unchanged during cyclic testing. However, the crack widths of the concrete link slab (~640 μm) at 100,000 loading cycles were substantially larger than those of the ECC link slabs (< 50 μm), by one order of magnitude. The tight crack width of ECC under cyclic loading will positively contribute to the durability of an ECC link slab and the potential realization of durable concrete deck systems as well. In terms of crack width limitations, the use of ECC, with crack widths and spacing as inherent material properties, will decouple the dependency of crack width on the amount of reinforcing bar, that is, the reinforcement ratio. This decoupling allows the simultaneous achievement of structural need (lower flexural stiffness of the link slab approaching the behavior of a hinge) and durability need (crack width control) of the link slab; and

5. There was no cracking observed at the interface between ECC link slab and RC deck slab during cyclic testing, while cracking formed over the debond span of the link slab up to the shear studs. This is due to the fact that the modified location of concrete/ECC interface as well as the additional shear studs installed in ECC link slab caused a shifting of the stress concentration from the concrete/ECC interface to the part of the ECC link slab. This modification is expected to provide enhanced integrity of the interface, preventing interfacial cracking.

The aforementioned conclusions support the contention that durable jointless concrete bridge decks may be designed and constructed with ECC link slabs.

ACKNOWLEDGMENTS

This work has been supported by a research grant from the Michigan Department of Transportation to the University of Michigan with project managers D. Juntunen (2001) and R. Till (2002-present). This support is gratefully acknowledged. M. Lepech, S. Wang, S. Qian, and M. Weimann contributed to this project.

REFERENCES

1. Wolde-Tinsae, A. M., and Klinger, J. E., "Integral Bridge Design and Construction," *Report* FHWA/MD-87/04, Maryland Department of Transportation, Jan. 1987.

2. Alampalli, S., and Yannotti, A. P., "In-Service Performance of Integral Bridges and Jointless Decks," *Transportation Research Record* 1624, Paper No. 98-0540, 1998, pp. 1-7.

3. Caner, A., and Zia, P., "Behavior and Design of Link Slab for Jointless Bridge Decks," *PCI Journal*, May-June 1998, pp. 68-80.

4. Li, V. C., "Reflections on the Research and Development of Engineered Cementitious Composites (ECC)," *Proceedings of the JCI International Workshop on Ductile Fiber Reinforced Cementitious Composites (DFRCC)—Application and Evaluation* (DFRCC-2002), Takayama, Japan, Oct. 2002, pp. 1-21.

5. Kong, H. J.; Bike, S.; and Li, V. C., "Constitutive Rheological Control to Develop a Self-Consolidating Engineered Cementitious Composite Reinforced with Hydrophilic Poly(vinyl alcohol) Fibers," *Cement and Concrete Composites*, V. 25, No. 3, 2003, pp. 333-341.

6. Kim, Y. Y.; Kong, H. J.; and Li, V. C., "Design of Engineered Cementitious Composite (ECC) Suitable for Wet-mix Shotcreting," *ACI Materials Journal*, V. 100, No. 6, Nov.-Dec. 2003, pp. 511-518.

7. Li, V. C., and Fischer, G., "Reinforced ECC—An Evolution from Materials to Structures," *Proceedings of the First FIB Congress*, Osaka, Japan, Oct. 2002, pp. 105-122.

8. AASHTO, "Standard Specifications for Highway Bridges," 17th Edition, American Association of State Highway and Transportation Officials, Washington D.C., 2002, 1052 pp.

9. Wang, K.; Jansen, D. C.; and Shah, S., "Permeability Study of Cracked Concrete," *Cement and Concrete Research*, V. 27, No. 3, 1997, pp. 381-393.

10. Weimann, M. B., and Li, V. C., "Hygral Behavior of Engineered Cementitious Composites (ECC)," *International Journal for Restoration of Buildings and Monuments*, V. 9, No. 5, 2003, pp. 513-534.

11. Gilani, A., and Juntunen, D., "Link Slabs for Simply Supported Bridges: Incorporating Engineered Cementitious Composites," *Report* No. MDOT SPR-54181, Michigan Department of Transportation, July 2001, 88 pp.

12. Fischer, G., and Li, V. C., "Influence of Matrix Ductility on Tension-Stiffening Behavior of Steel Reinforced Engineered Cementitious Composites (ECC)," *ACI Structural Journal*, V. 99, No. 1, Jan.-Feb. 2002, pp. 104-111.

13. Oesterle, R. G.; Tabatabai, H.; Lawson, T. J.; Refai, T. M.; Voltz, J. S.; and Scanlon, A., *Jointless and Integral Abutment Bridges—Summary Report*, Final Report to Federal Highway Administration, Washington D.C., 1999, 39 pp.